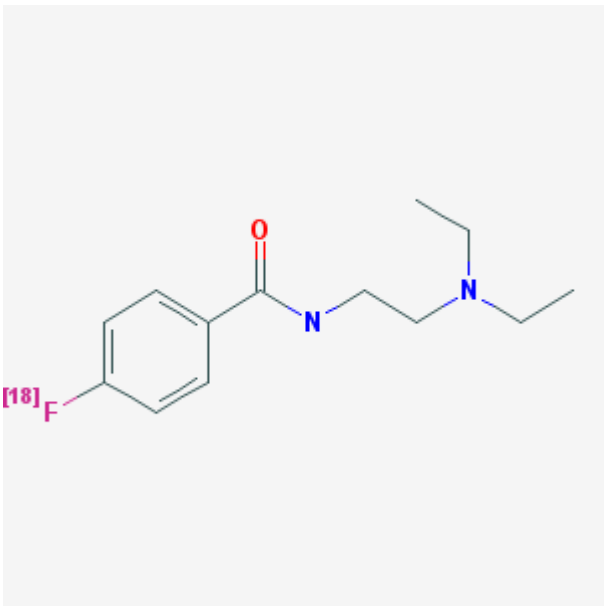


N-(2-Diethylaminoethyl)-4-¹⁸F fluorobenzamide for imaging melanoma

[¹⁸F]-DAFBA

Liang Shan, PhD¹

Created: November 19, 2009; Updated: December 30, 2009.

Chemical name:	<i>N</i> -(2-Diethylaminoethyl)-4-[¹⁸ F]fluorobenzamide for imaging melanoma	
Abbreviated name:	[¹⁸ F]-DAFBA	
Synonym:	¹⁸ F-FBZA	
Agent Category:	Compounds	
Target:	Melanin	
Target Category:	Others	
Method of detection:	Positron emission tomography (PET)	
Source of signal / contrast:	¹⁸ F	
Activation:		
Studies:	<ul style="list-style-type: none">• <i>In vitro</i>• Rodents	
		Click on the above structure for additional information in PubChem .

Background

[[PubMed](#)]

¹ National Center for Biotechnology Information, NLM, NIH; Email: micad@ncbi.nlm.nih.gov.

[✉] Corresponding author.

NLM Citation: Shan L. *N*-(2-Diethylaminoethyl)-4-[¹⁸F]fluorobenzamide for imaging melanoma. 2009 Nov 19 [Updated 2009 Dec 30]. In: Molecular Imaging and Contrast Agent Database (MICAD) [Internet]. Bethesda (MD): National Center for Biotechnology Information (US); 2004-2013.

Melanoma is one of the most deadly cancers in the United States. Although it accounts for only 4% of all skin cancer cases, melanoma is associated with ~79% of skin cancer-related deaths (1-3). The prognosis and the patient's survival depend heavily on the [clinical stage of the disease](#) at the time of diagnosis (4, 5). The 10-year survival rate for stage I melanoma patients is 90–97%, but only 3% for stage IV melanoma patients. Early detection and accurate assessment of the metastases remain the keys for improved outcome and disease-free survival. Unfortunately, the pattern of melanoma spread is often unpredictable, and conventional imaging with chest radiography, ultrasonography, computed tomography, and magnetic resonance imaging provides limited value for accurate staging and quantification of the disease burden (6, 7). Whole-body PET imaging with ^{18}F -labeled fluorodeoxyglucose (^{18}F FDG) has been shown to be superior to conventional imaging for detection of metastatic diseases, but it has not been shown to be useful for detecting small metastatic tumors (7, 8). Positive detection of nodal metastases requires nodal tumor involvement of more than 50% or capsular infiltration. Sub-centimeter pulmonary and hepatic metastases are frequently missed. Physiological uptake of FDG by the brain also limits its value in screening brain metastases. In an attempt to identify biomarkers of clinical utility, a large set of genes has been investigated for their abnormal expressions in melanoma (9-11). Potential biomarkers include p53, c-myc, CD44, Ki-67, Bcl-2, MITE, MMP2, p16, HIF2 α , CXCR4, CEACAM1, p-Akt, β 1 and β 3 integrins, tPA, ICAM1, ephrin A1, β -catenin, P-cadherin, pleiotropin, PLK-1, and PUMA (9-11). Although these biomarkers offer the possibility of improved tumor staging through the molecular detection of microscopic metastases, these studies have been hampered by the failure of individual biomarkers to provide significant prognostic information beyond the current staging system.

Benzamide derivatives represent a versatile class of compounds used as agents for molecular imaging, as transporters for cytostatic agents, and as inhibitors for histone deacetylases (12). Since *N*-(2-diethylaminoethyl)-4- ^{125}I iodobenzamide (^{125}I BZA) was first demonstrated to have high melanoma uptake, much effort has been made to further improve the affinity and pharmacological properties of this compound by modifying its structure such as using phenyl and amide substitutes (13, 14). Most benzamide derivatives possess the common structure element of $\text{Ph-CONH}(\text{CH}_2)_m\text{NR}_2$ ($m = 1,2$), and they exhibit comparable properties such as high melanoma uptake, which is a positive attribute for potentially useful imaging agents (12). The exact mechanism for the high melanoma uptake has not been fully established, although direct melanin binding, involvement in the melanin biosynthesis pathway, and sigma receptor mediation have been proposed as the most likely mechanisms for different derivatives. Garg et al. developed a radiolabeled benzamide derivative, *N*-(2-diethylaminoethyl) 4- ^{18}F fluorobenzamide (^{18}F -DAFBA), using the same structural motif of *N*-diethylaminoethyl-4- ^{123}I iodobenzamide (4- ^{123}I BZA) (1, 15). Garg et al. replaced the 4-iodo group of 4- ^{123}I BZA with a 4-fluoro group while keeping the remainder of the molecule unchanged. ^{18}F -DAFBA exhibited high melanoma uptake and low normal tissue retention. Their results suggest that ^{18}F -DAFBA could be a potentially useful

probe to image melanoma. Ren et al. synthesized and tested the same agent with the name of ¹⁸F-FBZA as a PET tracer (2).

Benzamide Derivatives-Related [Chapters in MICAD](#)

Synthesis

[PubMed]

Garg et al. detailed the synthetic procedures of native DAFBA and [¹⁸F]-DAFBA (1). The native DAFBA was prepared as a high-performance liquid chromatography (HPLC) reference standard for the production of [¹⁸F]-DAFBA, and it was synthesized with the reaction of 4-fluorobenzoic acid in dichloromethane with triethylamine and ethyl chloroformate for 1 h at 0°C. This reaction mixture was further reacted with *N,N*-diethylethylenediamine for 2 h at room temperature. The desired DAFBA was obtained with 84% yield and 98% chemical purity after HPLC. The radiochemical synthesis of [¹⁸F]-DAFBA was accomplished by first synthesizing 4-[¹⁸F]fluorobenzoic acid followed by its coupling to *N,N*-diethylethylenediamine. The 4-[¹⁸F]fluorobenzoic acid was prepared *via* two separate routes. For the first route, 4-[¹⁸F]fluorobenzaldehyde was prepared first, followed by oxidation of the aldehyde group to the carboxylic acid group. With this route, the 4-[¹⁸F]fluorobenzoic acid was synthesized with a $72 \pm 11\%$ radiochemical yield. For the second route, 4-[¹⁸F]fluorobenzoic acid was prepared in two steps, first by preparing ethyl-[¹⁸F]fluorobenzoate followed by hydrolyzing the ester group to yield 4-[¹⁸F]fluorobenzoic acid without isolating the intermediate ethyl ester. With the second route, the radiochemical yield of 4-[¹⁸F]fluorobenzoic acid was $82 \pm 8\%$ ($n = 11$). The coupling of *N,N*-diethylethylenediamine to 4-[¹⁸F]fluorobenzoic acid was accomplished with 1-(3-dimethylaminopropyl)-3-ethylcarbodiimide hydrochloride as the coupling agent. After coupling and purification, [¹⁸F]-DAFBA was obtained with $54 \pm 18\%$ radiochemical yield, $97 \pm 2\%$ radiochemical purity, and >37 GBq ($>1,000$ mCi)/ μmol specific activity. The overall synthesis time for [¹⁸F]-DAFBA, including HPLC purification and the final formulation, was 175 ± 15 min ($n = 17$). The radiochemical purity of [¹⁸F]-DAFBA remained $>95\%$ for up to 6 h after preparation of the product.

Ren et al. also described the synthesis of nonradioactive [¹⁹F]-DAFBA and radioactive [¹⁸F]-DAFBA under the names ¹⁹F-FBZA and ¹⁸F-FBZA, respectively (2). [¹⁹F]-DAFBA was synthesized in a one-step coupling reaction for 80 min at 50°C between *N,N*-diethylethylenediamine (DEDA) in dimethyl sulfoxide and *N*-succinimidyl-4-fluorobenzoate (SFB) in *N,N'*-diisopropylethylamine. After purification, the yield of [¹⁹F]-DAFBA was 70% and the measured molecular weight was 239.08 Da. Radiosynthesis of [¹⁸F]-DAFBA was achieved through coupling of ¹⁸F-SFB with the amino group of DEDA for 30 min at 50°C, followed by purification. The total radiosynthesis time for [¹⁸F]-DAFBA was 3 h, with an overall decay-corrected yield of 50% at the end of synthesis. The specific activity was estimated to be 132–166 GBq (3.57–4.49 Ci/ μmol), and the radiochemical purity was $>95\%$. The percentages of intact [¹⁸F]-DAFBA was 94.1%, 93.5%, 87.8%, and 85.1% at 30,

60, 120, and 150 min after incubation with mouse serum, respectively. Defluorination in mouse serum was not observed up to 150 min.

In Vitro Studies: Testing in Cells and Tissues

[PubMed]

Garg et al. analyzed the cell uptake of [^{18}F]-DAFBA in B16F1 mouse melanoma cells (1). The [^{18}F]-DAFBA uptake increased with increasing numbers of cultured cells, presenting an uptake of $5.60 \pm 2.67\%$ injected dose (ID) when 1×10^6 cells/tube were incubated with ~ 200 kcpm of [^{18}F]-DAFBA. The role of sigma receptors on the [^{18}F]-DAFBA cell uptake was then analyzed with competitive binding assay. For sigma-1 receptor binding, the assay was performed using the guinea pig brain membrane and the specific ligand ^3H -PENT. For sigma-2 receptor binding, the assay was performed using Sprague-Dawley rat liver membrane and the ligand ^3H -DTG. The results showed that sigma receptors were not implicated in the cell uptake of [^{18}F]-DAFBA. Because iodobenzamides with higher lipophilicity have been suggested to show better tumor uptake properties, and a $\log P_{7.4}$ of more than 1.4 is necessary for the enhanced tumor uptake characteristics, Garg et al. first calculated the $\log P$ value of [^{18}F]-DAFBA to be 2.01. They then measured the partition coefficient of [^{18}F]-DAFBA to be 1.7, a value similar to its calculated $\log P$ value. A higher lipophilicity (higher $\log P$) may enhance tissue penetration to improve tumor uptake, but it would simultaneously increase the nonspecific uptake in target and nontarget tissues. It is essential to carefully balance the physicochemical parameters when designing new probes.

Ren et al. also analyzed the cell uptake of [^{18}F]-DAFBA after 2 h incubation of 1×10^6 B16F10 murine melanoma cells with 3.7 kBq (0.1 μCi) [^{18}F]-DAFBA (2). Without pretreatment of the cells with L-tyrosine, the cell uptake after 2 h incubation was $0.49 \pm 0.03\%$ ID and $0.52 \pm 0.1\%$ ID at 4°C and 37°C , respectively. Pretreatment with L-tyrosine for 24 h significantly enhanced the cell uptake of [^{18}F]-DAFBA at both 4°C and 37°C ($P < 0.001$). At 37°C , uptake by the tyrosine-stimulated cells peaked at 30 min ($10.7 \pm 0.8\%$ ID), and the uptake remained at the level of $8.1 \pm 1.9\%$ ID at 2 h, an 18- to 25-fold increase compared with uptake by the nontreated B16F10 cells. Similar to the results obtained by Garg et al. (1), Ren et al. also showed that [^{19}F]-DAFBA displayed a low affinity for both the sigma-1 receptor (inhibition constant, 8.90 μmol) and the sigma-2 receptor (inhibition constant, 0.12 mmol).

Animal Studies

Rodents

[PubMed]

Garg et al. first investigated the biodistribution of [^{18}F]-DAFBA in ICR normal mice ($n = 20$) (1). In general, a low uptake was observed in most normal tissues over a 180-min study period. The kidneys and liver showed the highest uptake with $4.13 \pm 0.68\%$ ID/g for

the kidneys and $3.12 \pm 0.62\%$ ID/g for the liver at 30 min after injection. The radioactivity rapidly washed out from the kidneys and liver, approaching the levels seen in other normal tissues at 180 min (liver, $1.12 \pm 0.20\%$ ID/g; kidney, $1.34 \pm 0.36\%$ ID/g). Similar results were observed for the lungs, presenting radioactivity levels of $1.75 \pm 0.43\%$ ID/g at 30 min and $0.49 \pm 0.07\%$ ID/g at 180 min after injection. The radioactivity in blood was quite low at all time points, presenting $0.78 \pm 0.07\%$ and $0.21 \pm 0.03\%$ ID/g at 30 and 180 min after injection, respectively.

Garg et al. then investigated the tumor uptake of [¹⁸F]-DAFBA in C57 mice bearing B16F1 melanoma tumor allografts ($n = 20$) (1). The [¹⁸F]-DAFBA accumulation in the tumor-bearing mice was quite similar to that observed in the ICR normal mice. Most normal tissues had a low accumulation. In the tumor, [¹⁸F]-DAFBA displayed a rapid and high uptake. The tumor uptake reached $7.00 \pm 2.76\%$ ID/g by 60 min and decreased only slightly by 180 min ($5.80 \pm 0.98\%$ ID/g) with no statistical significance between the two time points ($P > 0.2$). The tumor uptake was also not dependent on the amount of radioactivity present in the blood pool ($r = 0.32$, $P > 0.05$). A high uptake in the tumor and low accumulation in the normal tissues resulted in a favorable tumor/normal tissue ratio. The tumor/blood ratio increased from 8.3 ± 3 at 60 min to 39 ± 12 at 180 min, a five-fold increase. Similarly, tumor/lung and tumor/muscle ratios were >20 at 180 min. [¹⁸F]-DAFBA crossed the blood–brain barrier within 30 min. After initial high uptake by the brain, the radioactivity rapidly decreased. The [¹⁸F]-DAFBA uptake in the normal brain was $2.02 \pm 0.35\%$ ID/g at 30 min and reduced to $0.29 \pm 0.05\%$ ID/g by 180 min, suggesting a low affinity of [¹⁸F]-DAFBA for normal brain tissue. Garg et al. concluded that rapid and high uptake of [¹⁸F]-DAFBA in tumor and low accumulation in normal tissues indicated its potential as a promising PET imaging probe to provide a high signal/noise ratio and an ability to clearly visualize tumors with low background signals (1). No blocking studies were reported.

Ren et al. performed biodistribution studies of [¹⁸F]-DAFBA in the subcutaneous and pulmonary metastasis models of B16F10 murine allografts as well as A375M and U87MG xenografts ($n = 3$ mice/group) (2). Amelanotic A375M human melanoma and U87MG human glioblastoma were used as control tumors. In the B16F10 subcutaneous tumor allografts (C57BL/6 mice), [¹⁸F]-DAFBA displayed a significant uptake being $6.47 \pm 2.16\%$ ID/g and $5.94 \pm 1.83\%$ ID/g at 1 h and 2 h after injection, respectively. The tumor/blood and tumor/muscle ratios reached 34.0 ± 13.2 and 23.3 ± 10.1 at 2 h after injection, respectively. In the A375M and U87MG mouse models (Nu/Foxn1 mice), however, the uptake in both A375M ($0.75 \pm 0.09\%$ ID/g) and U87MG ($0.56 \pm 0.13\%$ ID/g) xenografts was low, with tumor/blood ratios of 4.70 ± 0.78 and 3.57 ± 1.34 at 2 h after injection, respectively. For the B16F10 pulmonary metastasis model (C57BL/6 mice), animals were divided into two groups with 0.2×10^6 cells injected for the first group and 0.4×10^6 cells injected for the second group ($n = 3$ mice/group). The radioactivity in the lung with metastases reached $10.0 \pm 3.92\%$ ID/g for first group and $7.87 \pm 3.56\%$ ID/g for the second group at 2 h after injection. In the normal lung tissue, the probe accumulation was $0.99 \pm 0.04\%$ ID/g at 2 h after injection. The lung/blood ratios for the pulmonary metastasis model were 24.7 ± 13.5 and 38.9 ± 10.3 for the first and second groups,

respectively. The lung/blood ratios at 2 h were 4.72 ± 0.46 and 4.23 ± 0.66 for the B16F10 subcutaneous model and control C57BL/6 mice, respectively. Both absolute lung uptake and lung/blood ratio were significantly higher for the pulmonary metastasis model than for the subcutaneous model or for control C57BL/6 mice ($P < 0.01$). Small-animal PET imaging showed that the B16F10 tumors were clearly visualized at 1 h with a good tumor/background contrast, but A375M and U87MG tumors were not visualized well ($n = 3$ mice/group). B16F10 had a tumor uptake of $5.6 \pm 1.2\%$ ID/g, while A375M and U87MG had $0.86 \pm 0.03\%$ ID/g and $0.61 \pm 0.04\%$ ID/g ($P < 0.01$), respectively, suggesting specific binding of the [^{18}F]-DAFBA to melanin containing tumors. Liver and kidney uptake was visualized in all animals. The lung with metastasis, compared with the normal lung, clearly showed a region of symmetric uptake greater than the background level in the chest. Normal lung uptake of the [^{18}F]-DAFBA was $1.2 \pm 0.2\%$ ID/g, whereas uptake values of $10.2 \pm 0.1\%$ ID/g, $9.0 \pm 0.4\%$ ID/g, and $15.3 \pm 1.1\%$ ID/g were observed for lungs harboring metastases resulting from tumor doses of 0.2, 0.4, or 0.8×10^6 B16F10 cells, respectively. The total number of metastases and the metastatic tumor volume in the lungs were not described.

Ren et al. also performed a comparative analysis of [^{18}F]-DAFBA and ^{18}F -FDG in C57BL/6 mice with B16F10 allografts ($n = 3$ mice for [^{18}F]-DAFBA; $n = 5$ mice for ^{18}F -FDG) (2). The results showed that the uptake levels for the two agents in the B16F10 tumors at 1 h were not significantly different. The lung uptake values were $7.61 \pm 1.53\%$ ID/g and $2.92 \pm 0.40\%$ ID/g for ^{18}F -FDG and [^{18}F]-DAFBA, respectively, suggesting much higher normal-lung uptake of the ^{18}F -FDG ($P < 0.01$). Heart uptake of the ^{18}F -FDG was also significantly higher than that of the [^{18}F]-DAFBA ($P < 0.01$). However, liver uptake of the ^{18}F -FDG was lower than that of the [^{18}F]-DAFBA ($P < 0.05$).

Small-animal PET imaging of the B16F10 melanoma using [^{18}F]-DAFBA or ^{18}F -FDG showed that the two agents had different biodistribution patterns. High accumulation of the [^{18}F]-DAFBA was observed in the tumor and liver, and [^{18}F]-DAFBA was washed out through the kidneys. While high accumulation of the ^{18}F -FDG was observed in the heart, eyes (Harderian glands), and tumor, radioactivity in the liver was low. The tumor uptake was $5.6 \pm 1.2\%$ ID/g for [^{18}F]-DAFBA and $6.31 \pm 0.61\%$ ID/g for ^{18}F -FDG ($P > 0.05$). PET/computed tomography fusion images clearly demonstrated the tumor anatomy and specific tumor uptake of both probes. On the basis of their results, Ren et al. also concluded that [^{18}F]-DAFBA specifically targets primary and metastatic melanotic melanoma lesions with high tumor uptake and may have translational potential (2).

Other Non-Primate Mammals

[PubMed]

No references are currently available.

Non-Human Primates

[PubMed]

No references are currently available.

Human Studies

[PubMed]

No references are currently available.

References

1. Garg, S., K. Kothari, S.R. Thopate, A.K. Doke, and P.K. Garg, *Design, Synthesis, and Preliminary in Vitro and in Vivo Evaluation of N-(2-diethylaminoethyl)-4-[(18)F]fluorobenzamide ([18)F]-DAFBA): A Novel Potential PET Probe to Image Melanoma Tumors*. Bioconjug Chem, 2009
2. Ren G., Miao Z., Liu H., Jiang L., Limpa-Amara N., Mahmood A., Gambhir S.S., Cheng Z. *Melanin-targeted preclinical PET imaging of melanoma metastasis*. J Nucl Med. 2009;50(10):1692–9. PubMed PMID: 19759116.
3. Lens M. *Current clinical overview of cutaneous melanoma*. Br J Nurs. 2008;17(5):300–5. PubMed PMID: 18414292.
4. Mohr P., Eggermont A.M., Hauschild A., Buzaid A. *Staging of cutaneous melanoma*. Ann Oncol. 2009;20 Suppl 6:vi14–21. PubMed PMID: 19617293.
5. McLoughlin J.M., Zager J.S., Sondak V.K., Berk L.B. *Treatment options for limited or symptomatic metastatic melanoma*. Cancer Control. 2008;15(3):239–47. PubMed PMID: 18596676.
6. Choi E.A., Gershenwald J.E. *Imaging studies in patients with melanoma*. Surg Oncol Clin N Am. 2007;16(2):403–30. PubMed PMID: 17560520.
7. Kochhar, R., H. Ali, S. Mak, and P. Manoharan, *Metastatic cutaneous malignant melanoma: spectrum of imaging findings and the role of multimodality imaging*. J Med Imaging Radiat Oncol, 200953(5): p. 467-78; quiz 478-9.
8. Essner R., Belhocine T., Scott A.M., Even-Sapir E. *Novel imaging techniques in melanoma*. Surg Oncol Clin N Am. 2006;15(2):253–83. PubMed PMID: 16632214.
9. Gogas H., Eggermont A.M., Hauschild A., Hersey P., Mohr P., Schadendorf D., Spatz A., Dummer R. *Biomarkers in melanoma*. Ann Oncol. 2009;20 Suppl 6:vi8–13. PubMed PMID: 19617299.
10. Larson A.R., Konat E., Alani R.M. *Melanoma biomarkers: current status and vision for the future*. Nat Clin Pract Oncol. 2009;6(2):105–17. PubMed PMID: 19107110.
11. Rother J., Jones D. *Molecular markers of tumor progression in melanoma*. Curr Genomics. 2009;10(4):231–9. PubMed PMID: 19949544.
12. Oltmanns D., Eisenhut M., Mier W., Haberkorn U. *Benzamides as melanotropic carriers for radioisotopes, metals, cytotoxic agents and as enzyme inhibitors*. Curr Med Chem. 2009;16(17):2086–94. PubMed PMID: 19519383.
13. Michelot J.M., Moreau M.F., Labarre P.G., Madelmont J.C., Veyre A.J., Papon J.M., Parry D.F., Bonafous J.F., Boire J.Y., Desplanches G.G. et al. *Synthesis and evaluation of new iodine-125 radiopharmaceuticals as potential tracers for malignant melanoma*. J Nucl Med. 1991;32(8):1573–80. PubMed PMID: 1869982.

14. Mansard S., Papon J., Moreau M.F., Miot-Noirault E., Labarre P., Bayle M., Veyre A., Madelmont J.C., Moins N. *Uptake in melanoma cells of N-(2-diethylaminoethyl)-2-iodobenzamide (BZA2), an imaging agent for melanoma staging: relation to pigmentation.* Nucl Med Biol. 2005;32(5):451–8. PubMed PMID: 15982575.
15. Sillaire-Houtmann I., Bonafous J., Veyre A., Mestas D., D'Incan M., Moins N., Kemeny J.L., Chossat F., Bacin F. *J Fr Ophtalmol.* 2004;27(1):34–9. PubMed PMID: 14968075.